ACS OMEGA

http://pubs.acs.org/journal/acsodf

Article

Detecting Majorana Zero Modes via Strong Field Dynamics

Niccolò Baldelli,* Utso Bhattacharya, Daniel González-Cuadra, Maciej Lewenstein, and Tobias Graß

Cite This: *ACS Omega* 2022, 7, 47424−47430

Read Online

ACCESS | Metrics & More | Article Recommendations | Supporting Information

ABSTRACT: We propose a protocol to detect topological phase transitions of one-dimensional *p*-wave superconductors from their harmonic emission spectra in strong fields. Specifically, we identify spectral features due to radiating edge modes, which characterize the spectrum and the density of states in the topological phase and are absent in the trivial phase. These features allow us to define a measurable signature, obtained from emission measurements, that unambiguously differentiates between the two phases. Local probing provides insight into the localized and topologically protected nature of the modes. The presented results establish that high-harmonic spectroscopy can be used as an all-optical tool for the detection of Majorana zero modes.

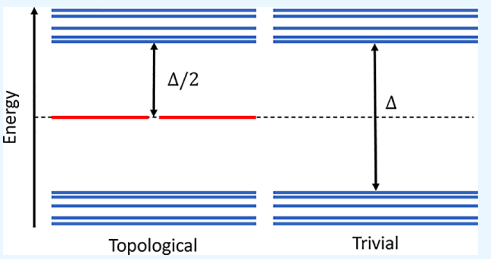

INTRODUCTION

The past decade has witnessed a hunt for the elusive Majorana fermions (MFs).[1] Although it is well-established that MFs can emerge as quasiparticles from condensed matter,[2] clear experimental evidence is still lacking. A paradigmatic system expected to host MFs at the edges is the one-dimensional (1D) spinless *p*-wave superconductor, also called a Kitaev chain.[3] In the topological superconducting state, the MFs appear as zero-energy modes in the middle of the superconducting gap and are therefore also called Majorana zero modes (MZMs). They are examples of symmetry-protected topological edge states,[4] and in two dimensions they possess non-Abelian anyonic statistics,[5] making them very interesting candidates for topological qubits thanks to their capability to robustly store and process quantum information.[6−8]

Despite the design of several experimental setups that effectively realize the Kitaev chain model,[9−18] the detection of MZMs remains challenging. In nanowire setups, MZMs are expected to appear as zero-energy states in the tunneling density-of-states (DOS), manifeting through a quantized zero-bias peak of height $2e^2/h$ in the differential conductance.[19−21] Despite several experiments showing compatible results,[22−24] there is still no conclusive evidence of the predicted robust quantization of the conductance.[25] Specifically, the zero-bias peaks are found at heights significantly smaller than $2e^2/h$, challenging their interpretation. Moreover, the observed nearly perfect conductance quantization may also stem from non-Majorana (nontopological) states.[26−28]

In this work, we develop an alternative approach for uncovering MZMs using the nonlinear response to strong sub-terahertz electromagnetic fields.[29] The strong fields bring the electrons into a nonperturbative regime in which their dynamics give rise to high-harmonic generation (HHG).[30] In the past, HHG has been used to track the dynamics of excitations at femtosecond time scales, yielding ultrafast imaging methods in atomic and molecular gases[31−34] and, more recently, in solid-state systems.[35−37] Lately, there has been increased interest in using HHG to detect topological properties of matter,[38−43] including MZMs in Kitaev chains.[44]

We improve on the previous work of ref 44 by considering a realistic system with *p*-wave superconductivity obtained via the proximity effect instead of studying an idealized toy model. This choice also allows us to address the coupling between the EM field and the electrons at a microscopic level, overcoming the ambiguity from the lack of gauge invariance of the Kitaev chain under minimal coupling with an EM field.

We show that the HHG spectrum of the system directly reflects the density of states and thus the widths of the energy bands and energy gaps. This gives rise to a spectroscopic scheme that distinguishes the topological phase from the trivial phase. Specifically, we introduce a measurable quantity, obtained from the HHG spectrum, that allows us to chart the whole phase diagram. Moreover, by focusing the radiation source to the edge, we are able to discern bulk excitations from edge excitations, clearly isolating the contribution from the topological MZMs. Our method can be used as an independent check for the presence of MZMs and, as an all-optical technique, can easily be applied to any sample without the need for gating, with a spatial resolution limited only by the wavelength of the light and a temporal resolution that enables the higher part of the excitation spectrum to be probed. Thus, it is suited to complementing or even substituting transport-

Received: November 7, 2022
Accepted: November 24, 2022
Published: December 7, 2022

https://doi.org/10.1021/acsomega.2c07169
ACS Omega 2022, 7, 47424−47430

based detection technique,[45] in order to provide the sought-after evidence of MZMs in condensed matter setups.

MODEL

The 1D p-wave superconducting Kitaev chain[3] is described by the Hamiltonian $H_K = \sum_n [-\mu c_n^\dagger c_n - t(c_{n+1}^\dagger c_n + \text{h. c. }) + \Delta(c_n c_{n+1} + \text{h. c. })]$, where $c_n^\dagger$ (c_n) is creation (annihilation) operator of spinless Fermions on site n. This model exhibits two phases, a trivial one and a topological one, with a topological phase transition at $|\mu| = 2t$. In the topological phase, for open boundary conditions, the spectrum is characterized by two degenerate ground states corresponding to MZMs localized at the two edges of the chain.

To study the response of this model to a strong field, the Fermions' coupling to the electromagnetic field is crucial. A naïve coupling to the vector potential $A(t)$ via the Peierls substitution, $c_j^\dagger \to e^{iAj} c_j^\dagger$, would require a corresponding dynamical change in the superconducting gap Δ to preserve the gauge-invariance of the Hamiltonian. While this is possible, we make the approximation that the value of Δ remains fixed throughout. Therefore, we focus on a particular system[11] that has been the main focus of recent experimental investigations and whose low-energy behavior is governed by the Kitaev chain Hamiltonian: a heterostructure between a semiconducting chain with strong spin−orbit coupling and a regular s-wave superconductor, which is additionally subjected to an external Zeeman field. Since the interactions with a strong field also excite high-energy states, we study the full multiband Hamiltonian of the heterostructure and not just its low-energy subspace. To capture the overall dynamics, we consider the time-dependent Hamiltonian for a chain of N sites in the Bogoliubov−de Gennes basis, $H = \Psi^\dagger H_{\text{BdG}} \Psi$, with

$$H_{\text{BdG}}(t) = \begin{pmatrix} J + I\frac{B}{2} & U(t) & I\Delta & 0 \\ U^\dagger(t) & J - I\frac{B}{2} & 0 & I\Delta \\ I\Delta^* & 0 & -J + I\frac{B}{2} & -U(t) \\ 0 & I\Delta^* & -U^*(t) & -J - I\frac{B}{2} \end{pmatrix} \tag{1}$$

Here, I is the $N \times N$ identity matrix and J and U are $N \times N$ matrices defined by $J_{l,m} = -\mu\delta_{l,m} + (\delta_{l,m-1} j e^{iA(t)} + \text{h.c.})$ and $U_{l,m}(t) = \delta_{l,m-1}\alpha e^{iA(t)} + \text{h.c.}$, respectively. The operator $\Psi^\dagger = (c_\uparrow^\dagger, c_\downarrow^\dagger, c_\downarrow, -c_\uparrow)$ is a "compressed" Nambu spinor, where $c_\sigma \equiv c_{1\sigma}, \ldots, c_{N\sigma}$, with $\sigma \in \{\uparrow, \downarrow\}$. The Hamiltonian's parameters are the hopping j, the chemical potential μ, the effective spin−orbit coupling α, the Zeeman field B, and the proximity-induced superconducting s-wave coupling Δ. In contrast to the Kitaev chain, this Hamiltonian lacks an explicit p-wave pairing term; therefore, the gauge-invariant coupling to the external field can be straightforwardly described via a Peierls substitution. For convenience, we choose units of $A(t)$ such that the coupling constant $ea/\hbar$, where a is the unit cell size, is 1. The time dependence of the vector potential is of the form

$$A(t) = A_0 \sin(\omega t) \sin^2\left(\frac{\omega t}{2n_c}\right) - \varepsilon_c t \quad 0 \le t \le 2\pi n_c/\omega \tag{2}$$

This describes a pulse of n_c cycles with frequency ω and a constant electric field with ε_c, explicitly breaking the time inversion symmetry in the system such that both even and odd harmonics of the driving frequency can be generated.[46] Measuring energies in units of j, we choose $\omega = 0.0025$ such that it corresponds roughly to 1/50 of the bandgap of the system. Specifically, to be able to discern the superconducting phase from a metallic phase, the driving frequency needs to be sufficiently smaller than the bandgap. The symmetry-breaking DC field is very weak, $\varepsilon_c = 10^{-5}$, whereas the amplitude of the vector potential has to be strong enough to produce high harmonics and is taken to be $A_0 = 1.2$, which for $a = 0.5$ nm corresponds to 1.6×10^{-6} Vs/m.

We note that our treatment makes the assumption that the light field only couples to the electrons of the semiconducting wire, while the pairing Δ from the surrounding superconductor is taken as a static parameter. This assumption is only justified if the superconductor is shielded from the incoming light.

For the static Hamiltonian at $t = 0$, the topological phase appears for $B > \sqrt{\Delta^2 + \mu^2}$.[47] For lower values of B, the system is in a trivial gapped superconducting state with no topological edge modes. We refer to the Supporting Information for a full derivation of the Hamiltonian. Although in realistic semiconductor−superconductor heterostructures the energy scales j, α, and Δ widely differ, in the following we choose them to be of the same order of magnitude (specifically, $\alpha = \Delta = 3/4$). The reason for this choice is to achieve clear Majorana modes for system sizes that are sufficiently small to numerically perform simulations of the full dynamics. In particular, the parameters were tuned according to the prescription from ref 48 in order to ensure the presence of a topological phase. For the purpose of detecting MZM from the high-harmonic spectrum, it is important that the ratio between the bandgap (usually on the order of Δ) and the frequency ω of the incoming pulse is much larger than 1. For InAs nanowires, the bandgap is on the order of 1 meV (with $j \sim 3000$ meV, $\alpha \sim 25$ meV, and $\Delta \sim B \sim \mu \sim 1$ meV, cf. ref 21), but much larger gaps have also been reported, such as 4 meV for β-Bi_2Pd films[49] or even 15 meV for iron-based superconductors.[50] Depending on the size of the gap, our scheme requires strong microwave to terahertz sources[29] with pulse duration son the order of 1−100 ps, which are potentially much shorter than typical relaxation time scales.

RESULTS AND DISCUSSION

The key quantity that captures the nonlinear optical response of the system is the transmitted HHG spectrum, that is, the normalized spectrum of emission

$$P(\omega) \propto |\text{FT}(\langle \dot{x} \rangle)|^2 / P_0 \tag{3}$$

where $P_0 = \max |\text{FT}[\partial_t A(t)]|^2$ is the maximum of the spectrum of the free incoming field,[51] which is $P_0 \sim 1.3 \times 10^{10}$ V^2/m^2 with our choice of parameters. Here, the time derivative of the average dipole moment $e\langle x(t) \rangle$ yields the electric current, which is Fourier transformed into the frequency domain. The dipole moment is calculated by numerically integrating the time-dependent Schrödinger equation (TDSE) from the initial

https://doi.org/10.1021/acsomega.2c07169
ACS Omega 2022, 7, 47424−47430

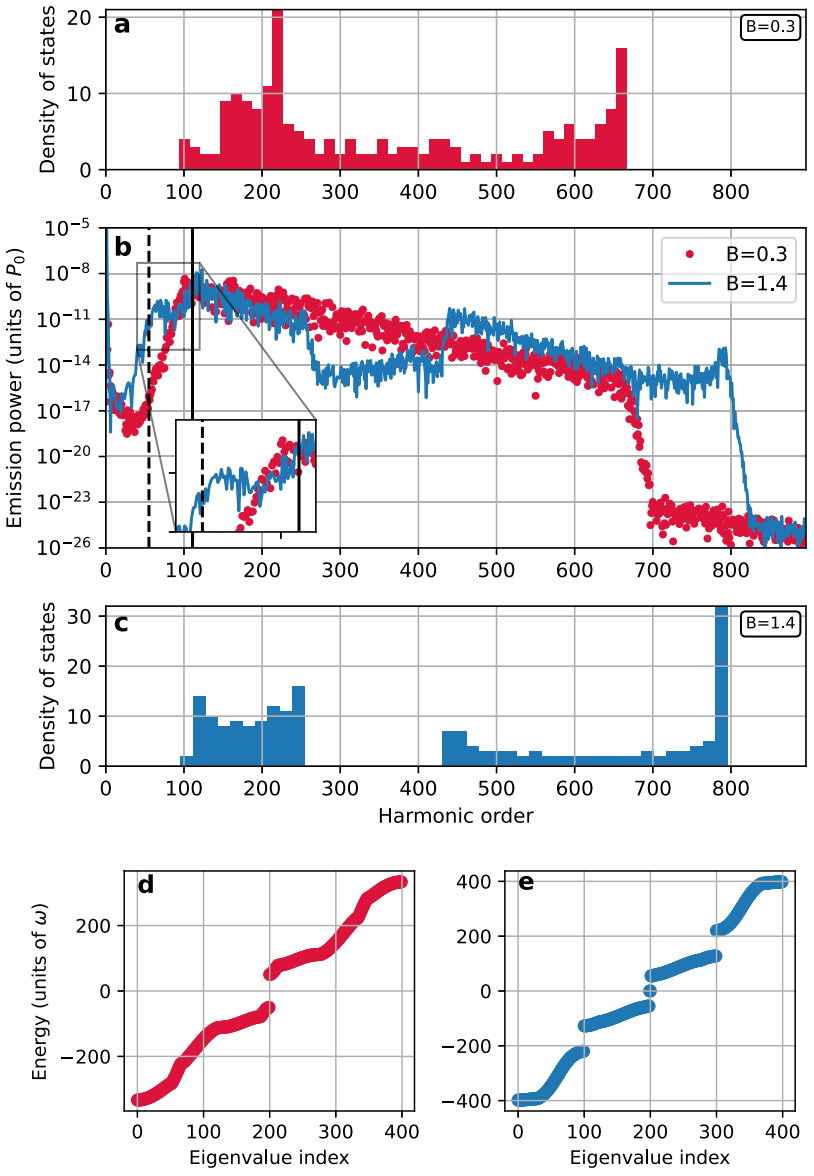

Figure 1. Comparison of the emitted spectrum deep in the topological (B = 1.4) and trivial (B = 0.3) phases for a spatially uniform field and μ = 0. The emission spectra shown in (b) follow the density of states of the Hamiltonian at time t = 0 in both (a) the trivial phase and (c) the topological phase. For the topological phase, an emission below the bandgap of the system (zoomed inset in (b)) can be related to the presence of zero-energy edge states. The density of states can be compared with the band structure in (d) the trivial phase and (e) the topological phase. Simulations were performed using parameters N = 100, ω = 0.0025, j = −0.3, α = Δ = 0.4, and A_0 = 1.2.

ground state of the Hamiltonian up to a time $T = 2\pi n_c/\omega$ (see the Supporting Information for details).

In Figure 1(b), we plot the emission spectrum, obtained from eq 3, as a function of the frequency of the emission in units of the driving frequency. We consider two points in parameter space, one deep in the trivial phase at B = 0.3 (red) and another in the topological phase at B = 1.4 (blue). Interestingly, in both cases, we observe that the spectrum echoes the band structure of the Bogoliubov Hamiltonian plotted in Figure 1(d) and (e), with two or four symmetric bands around the Fermi energy due to particle−hole symmetry.[48] In particular, the density of states in the two phases, shown in Figure 1(a) and (c), clearly determines the emission. In particular, there is no emission above the bandwidth or below the bandgap (defined as the difference between the highest valence band and the lowest conduction band excluding edge modes) in the trivial phase. In stark contrast, in the topological phase, the radiation plateau starts from half-bandgap, which is related to the presence of radiating edge modes at zero energy. For an explanation of this phenomenon, we refer to the Supporting Information.

For a qualitative understanding of the emission spectrum, we note that the dynamics that cause the emission can be split into three different steps:[30] (1) the incoming pulse can excite a Bogoliubov quasiparticle from the filled bands to the empty ones, (2) the excitation can then move inside the empty band under the applied electric field, and (3) it can subsequently relax back to one of the occupied bands. This leads to two different kinds of contributions in the emission spectrum, an intraband one (step 2) and an interband one (steps 1 and 3). The intraband contribution is produced by the acceleration (Bloch oscillations) of the quasiparticles within a band with nonlinear dispersion. The frequency of the interband emission, on the other hand, is bounded by the bandgap (lowest possible

https://doi.org/10.1021/acsomega.2c07169
ACS Omega 2022, 7, 47424−47430

interband excitation) and the bandwidth of the system (highest possible interband excitation). We note that for a short envelope, as considered here ($n_c = 5$), the Fourier transform of the incoming pulse is spread around the driving frequency. There is subsequently a widening and possible mixing of the harmonics generated by the system, but this is not of particular concern for our purposes, as we are not interested in discerning the emission at a particular frequency.

We now propose a measurable diagnostic, called contrast, defined as the ratio between the emission at half the bandgap P_{half} over the emission at the bandgap P_{gap}, which is on the order one in the topological phase and zero in the trivial phase.

$$C = \frac{\log(P_{\text{half}})}{\log(P_{\text{gap}})} \tag{4}$$

The choice of this quantity is dictated by the different behaviors of the emission at these special points in the two phases. The bandgap is defined as the minimum energy difference between the valence band and the conduction band, thus the minimum frequency at which emission can be produced by interband transitions in the trivial phase. The half-bandgap emission is chosen because this is where the edge states lie in the topological phase, leading to a possible interband transition to the conduction band that is impossible in the trivial phase. We refer to Figure 1 in the Supporting Information for a more exhaustive explanation.

The topological phase diagram of the system is computed in Figure 2 in the $\mu-B$ plane using the proposed signature.

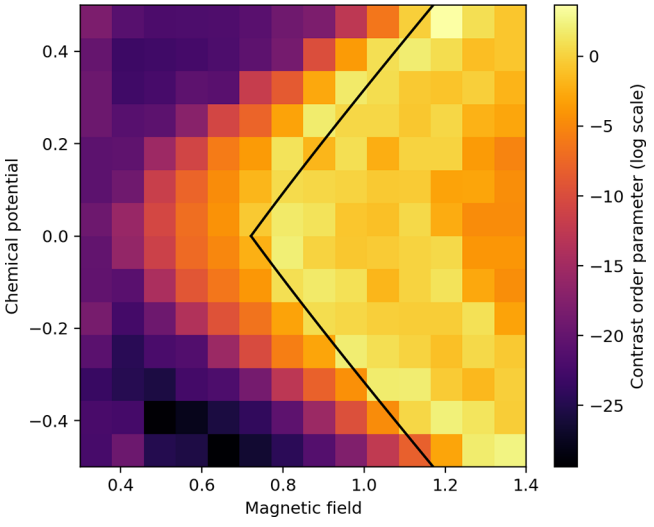

Figure 2. Contrast C as a function of the magnetic field and the chemical potential. In the topological phase $C \sim 1$, while in the trivial one $C \sim 0$. The black line represents the phase separation boundary for a system in the thermodynamic limit. Simulations were performed using parameters $N = 100$, $\omega = 0.0025$, $j = -0.3$, $\alpha = \Delta = 0.4$, and $A_0 = 1.2$.

Exactly at the boundary where the gap closes, the system behaves as a metal and the contrast is greater than one, as the emission is higher for lower harmonics. The choice of the frequency of the incident light pulse is crucial to localizing the phase boundary, as a lower frequency provides a sharper criterion for distinguishing topological and trivial phases. From this point of view, choosing a small driving frequency is favorable as long as the pulse remains short as compared to relaxation times; as the system approaches the transition, the gap closes, and when the driving frequency ω is of the order of the bandgap $\sim\Delta$, the response of the system becomes metallic. In this regime, the contrast order parameter is higher than 1 and generally not stable, as shown in Figure 3, where the bandgap deep in the trivial phase is $\sim\Delta = 0.4$. Therefore, a better resolution for detecting the phase transition is obtained when a lower driving frequency is chosen.

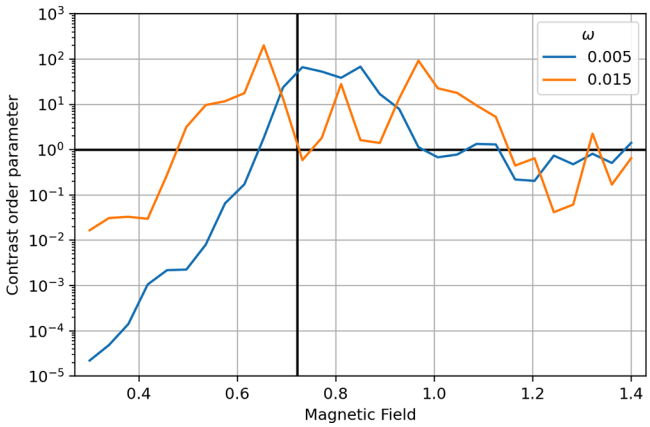

Figure 3. Contrast order parameter as a function of the magnetic field (at $\mu = 0$) for two values of the driving frequency. For the smaller frequency, the order parameter peaks at the phase boundary (indicated by the vertical black line) and quickly drops below 1 (indicated by the horizontal black line) in the trivial phase. For the larger frequency, the distinction between the phases is less sharp, and the order parameter overestimates the topological regime. Simulations were performed using parameters $N = 100$, $j = -0.3$, $\alpha = \Delta = 0.4$, $A_0 = 1.2$.

So far, the devised scheme distinguishes between topological and trivial phases by measuring the full bandstructure of the system, yet it does not capture the potentially most stunning property of the MZMs, that is, their localization at the edge and topological protection. However, with the spatial resolution of the radiation being limited only by the wavelength, it becomes possible to demonstrate that the sub-bandgap emission is due to edge modes by focusing the electromagnetic field on either the edge or the bulk of the sample. In Figure 4, we show how in the trivial phase the emitted spectrum is qualitatively the same for a pulse focused on the edge or on the bulk. On the other hand, in the topological phase, there is strong radiation between the bandgap and the half-bandgap if the light is focused on the edge, showing that the contribution to the emitted spectrum in this midbandgap region does not come from the bulk but solely from the edge. We have used a Gaussian envelope, which was cut in half for the edge radiation, and the amplitude of the envelopes was normalized in order to have the same total energy of the electromagnetic field for all cases (edge, bulk, and uniform field).

Finally, to illustrate the topological nature of the edge modes, we add a local perturbation to the system that does not break the particle−hole symmetry of the Hamiltonian. Such local potentials (acting on three sites on the left and right edges) can be added by applying gate voltages at the edges and are modeled by adding a term $jl_p \sum_{i,\sigma} c_{i\sigma}^{\dagger} c_{i\sigma}$ for $i = 1, 2, 3, N-2, N-1, N$. We observe that increasing the value of this potential does not affect the shape of the emission spectrum.

https://doi.org/10.1021/acsomega.2c07169
ACS Omega 2022, 7, 47424−47430

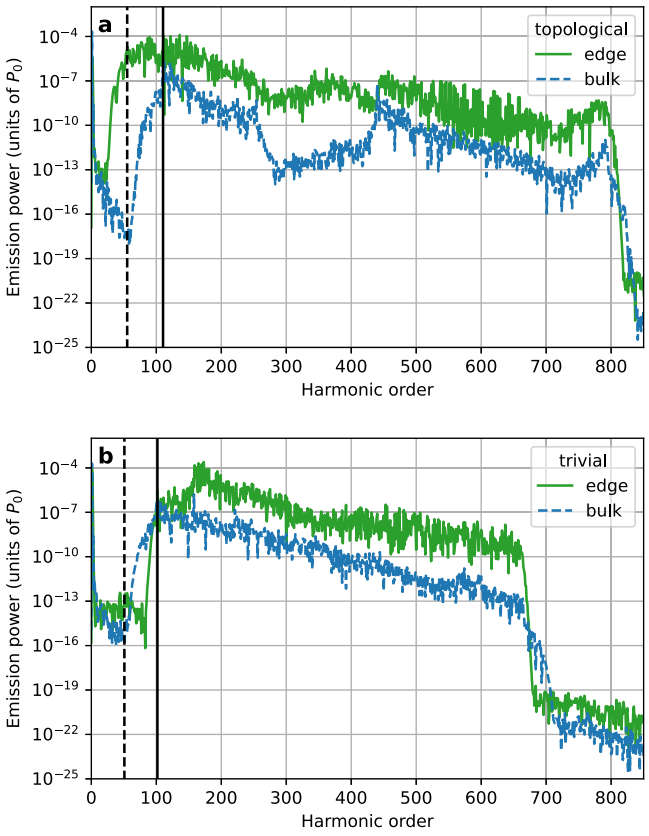

Figure 4. Emission for a pulse focused on the edge or the bulk of the sample in (a) the topological phase and (b) the trivial phase. The spacial envelope is normalized to have constant energy of the EM field. In the topological phase, the spectra differ depending on where the pulse is focused, showing emission from sub-bandgap states only when the pulse is focused on the edge. This is not the case, however, in the trivial phase, where both spectra are qualitatively similar. Simulations were performed using parameters $N = 100$, $\omega = 0.0025$, $j = -0.3$, $\alpha = \Delta = 0.4$, and $A_0 = 1.2$.

Specifically, the sub-bandgap edge-state emission only appears in the topological phase and remains present precisely between the half-bandgap and the bandgap, as can be seen in Figure 5. The different curves in this figure, corresponding to different edge potentials, lie on top of each other for lower harmonics (until the bandgap of the system), indicating that the edge modes do not shift in energy upon the application of edge potentials and clearly demonstrating the topological robustness of the radiating edge modes.

CONCLUSION

In the present article, topological edge modes are detected via the electromagnetic emission spectrum in the nonlinear regime. An experimentally observable quantity, the contrast, is constructed to map the phase diagram. To confirm the topological nature of radiating modes, the system can be probed locally and shown to be robust under local perturbations. Thus, our protocol complements other established methods in the pursuit of MZMs.

A major experimental challenge for the detection of MZMs is distinguishing them from trivial sub-bandgap states that can appear in the material, that is, Andreev bound states.[52−55] These states can appear from regions in the semiconducting chain where the proximity-induced superconductivity fails (i.e., near the edges), creating zones of normal metal where

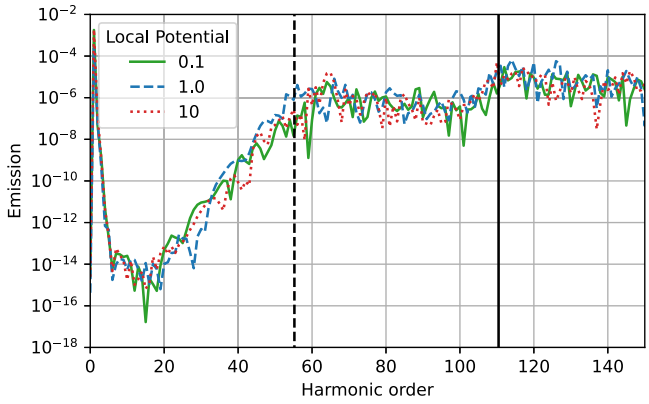

Figure 5. Emission spectra with the addition of a local potential on the edges of the chain (in units of j). The local potential acts on the first and last three sites and does not break the symmetry responsible for the topological protection. The qualitative behavior of the emission of the edge states does not change as the value of this potential increases. The black lines indicate the half bandgap and the bandgap in the order of the driving frequency. Simulations were performed using parameters $N = 100$, $\omega = 0.0025$, $j = -0.3$, $\alpha = \Delta = 0.4$, and $A_0 = 1.2$.

scattering effects can lead to the creation of localized states.[56] A straightforward extension of our work will use a spatially dependent superconducting order parameter to study the formation of these states and their influence on the emission spectrum. Another interesting application of our technique is the study of Majorana physics in two dimensions, where MZMs can arise as vortices in p-wave superconductors.[57] Compared to 1D models, the dependence of the emission spectrum on the field polarization states will make the two-dimensional scenario very rich. Recent studies have shown that left−right polarized drives can shed light on the presence of topological chiral states[58,59] in both the perturbative and ultrastrong regime,[41,42] but a study of the effect on Majoranas is still missing.

ASSOCIATED CONTENT

Supporting Information

The Supporting Information is available free of charge at https://pubs.acs.org/doi/10.1021/acsomega.2c07169.

Derivation of the nanowire Hamiltonian and description of the numerical techniques used (PDF)

AUTHOR INFORMATION

Corresponding Author

Niccolò Baldelli − *Institut de Ciencies Fotoniques (ICFO), The Barcelona Institute of Science and Technology, 08860 Castelldefels, Barcelona, Spain;* orcid.org/0000-0003-4352-0041; Email: niccolo.baldelli@icfo.eu

Authors

Utso Bhattacharya − *Institut de Ciencies Fotoniques (ICFO), The Barcelona Institute of Science and Technology, 08860 Castelldefels, Barcelona, Spain;* orcid.org/0000-0002-1447-443X

Daniel González-Cuadra − *Institut de Ciencies Fotoniques (ICFO), The Barcelona Institute of Science and Technology, 08860 Castelldefels, Barcelona, Spain; Institute for Theoretical Physics, University of Innsbruck, 6020 Innsbruck, Austria; Institute for Quantum Optics and Quantum*

https://doi.org/10.1021/acsomega.2c07169
ACS Omega 2022, 7, 47424−47430

Information, Austrian Academy of Sciences, 6020 Innsbruck, Austria

Maciej Lewenstein − *Institución Catalana de Investigación y Esteudios Avanzados (ICREA), 08010 Barcelona, Barcelona, Spain; Institut de Ciencies Fotoniques (ICFO), The Barcelona Institute of Science and Technology, 08860 Castelldefels, Barcelona, Spain*

Tobias Graß − *Institut de Ciencies Fotoniques (ICFO), The Barcelona Institute of Science and Technology, 08860 Castelldefels, Barcelona, Spain; Donostia International Physics Center (DIPC), 20018 San Sebastián, Gipuzkoa, Spain; Ikerbasque, 48013 Bilbao, Biscay, Spain;* orcid.org/0000-0002-8163-9353

Complete contact information is available at: https://pubs.acs.org/10.1021/acsomega.2c07169

Notes

The authors declare no competing financial interest.

■ ACKNOWLEDGMENTS

We thank A. Dauphin, A. Maxwell, J.-M. Raimond, and P. Stammer for useful discussions and insightful comments The . ICFO group acknowledges support from ERC AdG NOQIA; Agencia Estatal de Investigación (R&D project CEX2019-000910-S, funded by MCIN/AEI/10.13039/501100011033, Plan National FIDEUA PID2019-106901GB-I00, FPI, QUANTERA MAQS PCI2019-111828-2, Proyectos de I+D+I "Retos Colaboración" QUSPIN RTC2019-007196-7); Fundació Cellex; Fundació Mir-Puig; Generalitat de Catalunya through the European Social Fund FEDER and CERCA program (AGAUR Grant 2017 SGR 134, QuantumCAT U16-011424, cofunded by ERDF Operational Program of Catalonia 2014-2020); EU Horizon 2020 FET-OPEN OPTOlogic (Grant 899794); National Science Centre, Poland (Symfonia Grant 2016/20/W/ST4/00314); and European Union's Horizon 2020 research and innovation program under Marie-Skłodowska-Curie Grants 101029393 (STREDCH) and 847648 ("La Caixa" Junior Leaders fellowships ID100010434 LCF/BQ/PI19/11690013, LCF/BQ/PI20/11760031, LCF/BQ/PR20/11770012, and LCF/BQ/PR21/11840013). N.B. acknowledges support from a "la Caixa" Foundation (ID 100010434) fellowship. The fellowship code is LCF/BQ/DI20/11780033. T.G. acknowledges financial support from a fellowship granted by "la Caixa" Foundation (ID 100010434, fellowship code LCF/BQ/PI19/11690013). D.G.-C. is supported by the Simons Collaboration on Ultra-Quantum Matter, which is a grant from the Simons Foundation (651440, P.Z.).

■ REFERENCES

(1) Majorana, E. Teoria simmetrica dell'elettrone e del positrone. *Nuovo Cim* **1937**, *14*, 171.
(2) Wilczek, F. Majorana returns. *Nat. Phys.* **2009**, *5*, 614−618.
(3) Kitaev, A. Y. Unpaired Majorana fermions in quantum wires. *Phys.-Uspekhi* **2001**, *44*, 131−136.
(4) Chiu, C.-K.; Teo, J. C. Y.; Schnyder, A. P.; Ryu, S. Classification of topological quantum matter with symmetries. *Rev. Mod. Phys.* **2016**, *88*, 035005.
(5) Stern, A. Non-Abelian states of matter. *Nature* **2010**, *464*, 187−193.
(6) Kitaev, A. Fault-tolerant quantum computation by anyons. *Ann. Phys. (N. Y.)* **2003**, *303*, 2−30.
(7) Sarma, S. D.; Freedman, M.; Nayak, C. Majorana zero modes and topological quantum computation. *npj Quantum Inf.* **2015**, *1*, 15001.
(8) Alicea, J.; Oreg, Y.; Refael, G.; von Oppen, F.; Fisher, M. P. A. Non-Abelian statistics and topological quantum information processing in 1D wire networks. *Nat. Phys.* **2011**, *7*, 412−417.
(9) Fu, L.; Kane, C. L. Superconducting Proximity Effect and Majorana Fermions at the Surface of a Topological Insulator. *Phys. Rev. Lett.* **2008**, *100*, 096407.
(10) Fu, L.; Kane, C. L. Josephson current and noise at a superconductor/quantum-spin-Hall-insulator/superconductor junction. *Phys. Rev. B* **2009**, *79*, 161408.
(11) Oreg, Y.; Refael, G.; von Oppen, F. Helical Liquids and Majorana Bound States in Quantum Wires. *Phys. Rev. Lett.* **2010**, *105*, 177002.
(12) Lutchyn, R. M.; Sau, J. D.; Das Sarma, S. Majorana Fermions and a Topological Phase Transition in Semiconductor-Superconductor Heterostructures. *Phys. Rev. Lett.* **2010**, *105*, 077001.
(13) Cook, A.; Franz, M. Majorana fermions in a topological-insulator nanowire proximity-coupled to an *s*-wave superconductor. *Phys. Rev. B* **2011**, *84*, 201105.
(14) Kemp, J.; Yao, N. Y.; Laumann, C. R.; Fendley, P. Long coherence times for edge spins. *Journal of Statistical Mechanics: Theory and Experiment* **2017**, *2017*, 063105.
(15) Wang, Y. Detecting topological phases via survival probabilities of edge Majorana fermions. *Phys. Rev. E* **2018**, *98*, 042128.
(16) Gómez-Ruiz, F. J.; Mendoza-Arenas, J. J.; Rodríguez, F. J.; Tejedor, C.; Quiroga, L. Universal two-time correlations, out-of-time-ordered correlators, and Leggett-Garg inequality violation by edge Majorana fermion qubits. *Phys. Rev. B* **2018**, *97*, 235134.
(17) Dağ, C. B.; Duan, L.-M.; Sun, K. Topologically induced prescrambling and dynamical detection of topological phase transitions at infinite temperature. *Phys. Rev. B* **2020**, *101*, 104415.
(18) Bjerlin, J.; Sørensen, A. S.; Haas, S. Probing Majorana modes via local spin dynamics. *Phys. Rev. B* **2022**, *106*, 035414.
(19) Law, K. T.; Lee, P. A.; Ng, T. K. Majorana Fermion Induced Resonant Andreev Reflection. *Phys. Rev. Lett.* **2009**, *103*, 237001.
(20) Flensberg, K. Tunneling characteristics of a chain of Majorana bound states. *Phys. Rev. B* **2010**, *82*, 180516.
(21) Stanescu, T. D.; Lutchyn, R. M.; Das Sarma, S. Majorana fermions in semiconductor nanowires. *Phys. Rev. B* **2011**, *84*, 144522.
(22) Mourik, V.; Zuo, K.; Frolov, S. M.; Plissard, S. R.; Bakkers, E. P. A. M.; Kouwenhoven, L. P. Signatures of Majorana Fermions in Hybrid Superconductor-Semiconductor Nanowire Devices. *Science* **2012**, *336*, 1003−1007.
(23) Deng, M. T.; Yu, C. L.; Huang, G. Y.; Larsson, M.; Caroff, P.; Xu, H. Q. Anomalous Zero-Bias Conductance Peak in a Nb−InSb Nanowire−Nb Hybrid Device. *Nano Lett.* **2012**, *12*, 6414−6419.
(24) Das, A.; Ronen, Y.; Most, Y.; Oreg, Y.; Heiblum, M.; Shtrikman, H. Zero-bias peaks and splitting in an Al−InAs nanowire topological superconductor as a signature of Majorana fermions. *Nat. Phys.* **2012**, *8*, 887−895.
(25) Yu, P.; Chen, J.; Gomanko, M.; Badawy, G.; Bakkers, E. P. A. M.; Zuo, K.; Mourik, V.; Frolov, S. M. Non-Majorana states yield nearly quantized conductance in proximatized nanowires. *Nat. Phys.* **2021**, *17*, 482−488.
(26) Liu, J.; Potter, A. C.; Law, K. T.; Lee, P. A. Zero-Bias Peaks in the Tunneling Conductance of Spin-Orbit-Coupled Superconducting Wires with and without Majorana End-States. *Phys. Rev. Lett.* **2012**, *109*, 267002.
(27) Lee, E. J. H.; Jiang, X.; Aguado, R.; Katsaros, G.; Lieber, C. M.; De Franceschi, S. Zero-Bias Anomaly in a Nanowire Quantum Dot Coupled to Superconductors. *Phys. Rev. Lett.* **2012**, *109*, 186802.
(28) Das Sarma, S.; Pan, H. Disorder-induced zero-bias peaks in Majorana nanowires. *Phys. Rev. B* **2021**, *103*, 195158.
(29) Hafez, H. A.; Kovalev, S.; Deinert, J.-C.; Mics, Z.; Green, B.; Awari, N.; Chen, M.; Germanskiy, S.; Lehnert, U.; Teichert, J.; et al. Extremely efficient terahertz high-harmonic generation in graphene by hot Dirac fermions. *Nature* **2018**, *561*, 507−511.

(30) Vampa, G.; McDonald, C. R.; Orlando, G.; Klug, D. D.; Corkum, P. B.; Brabec, T. Theoretical Analysis of High-Harmonic Generation in Solids. *Phys. Rev. Lett.* **2014**, *113*, 073901.
(31) Krause, J. L.; Schafer, K. J.; Kulander, K. C. High-order harmonic generation from atoms and ions in the high intensity regime. *Phys. Rev. Lett.* **1992**, *68*, 3535−3538.
(32) Krausz, F.; Ivanov, M. Attosecond physics. *Rev. Mod. Phys.* **2009**, *81*, 163−234.
(33) Baker, S.; Robinson, J. S.; Haworth, C. A.; Teng, H.; Smith, R. A.; Chiril ă, C. C.; Lein, M.; Tisch, J. W. G.; Marangos, J. P. Probing Proton Dynamics in Molecules on an Attosecond Time Scale. *Science* **2006**, *312*, 424−427.
(34) Shafir, D.; Soifer, H.; Bruner, B. D.; Dagan, M.; Mairesse, Y.; Patchkovskii, S.; Ivanov, M. Y.; Smirnova, O.; Dudovich, N. Resolving the time when an electron exits a tunnelling barrier. *Nature* **2012**, *485*, 343−346.
(35) Hohenleutner, M.; Langer, F.; Schubert, O.; Knorr, M.; Huttner, U.; Koch, S. W.; Kira, M.; Huber, R. Real-time observation of interfering crystal electrons in high-harmonic generation. *Nature* **2015**, *523*, 572−575.
(36) Ghimire, S.; Reis, D. A. High-harmonic generation from solids. *Nat. Phys.* **2019**, *15*, 10−16.
(37) Alcalà, J.; Bhattacharya, U.; Biegert, J.; Ciappina, M.; Elu, U.; Graß, T.; Grochowski, P. T.; Lewenstein, M.; Palau, A.; Sidiropoulos, T. P. H.; Steinle, T.; Tyulnev, I.High harmonic spectroscopy of quantum phase transitions in a high-T_c superconductor. *arXiv (Condensed Matter.Superconductivity)*, January 24, 2022, 2201.09515, ver. 1. DOI: 10.48550/arXiv.2201.09515.
(38) Reimann, J.; Schlauderer, S.; Schmid, C.; Langer, F.; Baierl, S.; Kokh, K.; Tereshchenko, O.; Kimura, A.; Lange, C.; Güdde, J.; et al. Subcycle observation of lightwave-driven Dirac currents in a topological surface band. *Nature* **2018**, *562*, 396−400.
(39) Bauer, D.; Hansen, K. K. High-Harmonic Generation in Solids with and without Topological Edge States. *Phys. Rev. Lett.* **2018**, *120*, 177401.
(40) Jürß, C.; Bauer, D. High-harmonic generation in Su-Schrieffer-Heeger chains. *Phys. Rev. B* **2019**, *99*, 195428.
(41) Silva, R. E. F.; Jiménez-Galán, Á.; Amorim, B.; Smirnova, O.; Ivanov, M. Topological strong-field physics on sub-laser-cycle timescale. *Nat. Photonics* **2019**, *13*, 849−854.
(42) Chacón, A.; Kim, D.; Zhu, W.; Kelly, S. P.; Dauphin, A.; Pisanty, E.; Maxwell, A. S.; Picón, A.; Ciappina, M. F.; Kim, D. E.; et al. Circular dichroism in higher-order harmonic generation: Heralding topological phases and transitions in Chern insulators. *Phys. Rev. B* **2020**, *102*, 134115.
(43) Shao, C.; Lu, H.; Zhang, X.; Yu, C.; Tohyama, T.; Lu, R. High-Harmonic Generation Approaching the Quantum Critical Point of Strongly Correlated Systems. *Phys. Rev. Lett.* **2022**, *128*, 047401.
(44) Pattanayak, A.; Pujari, S.; Dixit, G. Role of Majorana fermions in high-harmonic generation from Kitaev chain. *Sci. Rep.* **2022**, *12*, 6722.
(45) Law, K. T.; Lee, P. A.; Ng, T. K. Majorana Fermion Induced Resonant Andreev Reflection. *Phys. Rev. Lett.* **2009**, *103*, 237001.
(46) Kanega, M.; Ikeda, T. N.; Sato, M. Linear and nonlinear optical responses in Kitaev spin liquids. *Phys. Rev. Res.* **2021**, *3*, L032024.
(47) Leijnse, M.; Flensberg, K. Introduction to topological superconductivity and Majorana fermions. *Semicond. Sci. Technol.* **2012**, *27*, 124003.
(48) Alicea, J. New directions in the pursuit of Majorana fermions in solid state systems. *Rep. Prog. Phys.* **2012**, *75*, 076501.
(49) Guan, J.-Y.; Kong, L.; Zhou, L.-Q.; Zhong, Y.-G.; Li, H.; Liu, H.-J.; Tang, C.-Y.; Yan, D.-Y.; Yang, F.-Z.; Huang, Y.-B.; Shi, Y.-G.; Qian, T.; Weng, H.-M.; Sun, Y.-J.; Ding, H. Experimental evidence of anomalously large superconducting gap on topological surface state of β-Bi_2Pd film. *Sci. Bull.* **2019**, *64*, 1215−1221.
(50) Hagiwara, K.; Ishikado, M.; Horio, M.; Koshiishi, K.; Nakata, S.; Ideta, S.; Tanaka, K.; Horiba, K.; Ono, K.; Kumigashira, H.; Yoshida, T.; Ishida, S.; Eisaki, H.; Shamoto, S.; Fujimori, A. Superconducting gap and pseudogap in the surface states of the iron-based superconductor $PrFeAsO_{1-y}$ studied by angle-resolved photoemission spectroscopy. *Phys. Rev. Res.* **2021**, *3*, 043151.
(51) Baggesen, J. C.; Madsen, L. B. On the dipole, velocity and acceleration forms in high-order harmonic generation from a single atom or molecule. *J. Phys. B At. Mol. Opt.* **2011**, *44*, 115601.
(52) Sauls, J. Andreev bound states and their signatures. *Philos. Trans. R. Soc. A* **2018**, *376*, 20180140.
(53) Tuovinen, R.; Perfetto, E.; van Leeuwen, R.; Stefanucci, G.; Sentef, M. A. Distinguishing Majorana zero modes from impurity states through time-resolved transport. *New J. Phys.* **2019**, *21*, 103038.
(54) Prada, E.; San-Jose, P.; de Moor, M. W. A.; Geresdi, A.; Lee, E. J. H.; Klinovaja, J.; Loss, D.; Nygård, J.; Aguado, R.; Kouwenhoven, L. P. From Andreev to Majorana bound states in hybrid superconductor−semiconductor nanowires. *Nat. Rev. Phys.* **2020**, *2*, 575−594.
(55) Tanaka, Y.; Tamura, S. Theory of Surface Andreev Bound States and Odd-Frequency Pairing in Superconductor Junctions. *Journal of Superconductivity and Novel Magnetism* **2021**, *34*, 1677−1694.
(56) Andreev, A. Thermal conductivity of the intermediate state in superconductors. *Sov. Phys. JETP* **1964**, *19* (5), 1228−1231.
(57) Read, N.; Green, D. Paired states of fermions in two dimensions with breaking of parity and time-reversal symmetries and the fractional quantum Hall effect. *Phys. Rev. B* **2000**, *61*, 10267−10297.
(58) Tran, D. T.; Dauphin, A.; Grushin, A. G.; Zoller, P.; Goldman, N. Probing topology by "heating": Quantized circular dichroism in ultracold atoms. *Sci. Adv.* **2017**, *3*, No. e1701207.
(59) Asteria, L.; Tran, D. T.; Ozawa, T.; Tarnowski, M.; Rem, B. S.; Fläschner, N.; Sengstock, K.; Goldman, N.; Weitenberg, C. Measuring quantized circular dichroism in ultracold topological matter. *Nat. Phys.* **2019**, *15*, 449−454.

https://doi.org/10.1021/acsomega.2c07169
ACS Omega 2022, 7, 47424−47430